Journal of Power Sources 196 (2011) 5751–5755

Contents lists available at ScienceDirect

Journal of Power Sources

journal homepage: www.elsevier.com/locate/jpowsour

Short communication

Structure and electrochemical properties of ball-milled Co-carbon nanotube composites as negative electrode material of alkaline rechargeable batteries

Hongmei Du, Lifang Jiao*, Qinghong Wang, Wenxiu Peng, Dawei Song, Yijing Wang, Huatang Yuan

Institute of New Energy Material Chemistry, Key Laboratory of Advanced Energy Materials Chemistry (MOE), MOE (IRT-0927), Nankai University, 94 Weijin Road, Tianjin 300071, PR China

ARTICLE INFO

Article history:
Received 15 November 2010
Accepted 26 November 2010
Available online 2 December 2010

Keywords:
Co-carbon nanotube composites
Ball-milling
Electrochemical performance
Faradaic redox
Alkaline rechargeable battery
Negative electrode

ABSTRACT

A series of cobalt-carbon nanotube (CNT) composites is synthesized by direct ball-milling of Co and CNT powders with different Co/CNT weight ratios. The microstructure, morphology and chemical state of the ball-milled Co-CNT composites are characterized by X-ray diffraction (XRD), transmission electron microscopy (TEM) and X-ray photoelectron spectroscopy (XPS). It is found that metallic Co nanoparticles of 50–100 nm in size are highly dispersed on the inactive CNT matrix after ball-milling. The electrochemical performance of Co-CNT composites as negative electrode material of alkaline rechargeable batteries is investigated by galvanostatic charge–discharge, linear polarization and cyclic voltammetry (CV) techniques. The results show that the Co-CNT composite (weight ratio 5/1, BM 10 h) displays the optimized electrochemical performance, including discharge capacity and cycle stability. The reversible faradaic reaction between Co and $Co(OH)_2$ is dominant for ball-milled Co-CNT composites.

1. Introduction

As we all know, cobalt metal and its compounds are widely used as resources in energy storage and conversion apparatus, such as in Ni-metal hydride (Ni-MH) batteries, lithium ion batteries and proton exchange membrane fuel cells [1–3]. Nowadays, extensive research has been focused on cobalt based alloys as negative materials for alkaline rechargeable batteries, such as Co–B, Co–P, Co–Si, Co–BN, Co–Si_3N_4 [4–11] and so on, which are demonstrated to have a good electrochemical reversibility and high charge–discharge capacities. In these reports, through ball-milling or chemical methods, little Co particles with good reaction activity distribute well among non-metallic matrix. Besides, the amorphous structure after treatment is more effective for the enhanced utilization due to fast transport of active species compared to crystalline structures. These factors all contribute to the enhanced utilization of metallic cobalt in the oxidation reaction. In general, the cobalt element exists as metallic Co, $Co(OH)_2$ and CoOOH in alkaline solution, depending on the potential range [12,13]. Elumalai et al. reported that the pair of current peaks close to the hydrogen evolution reaction (HER) was caused by the quasi-reversible reduction and oxidation between $Co(OH)_2$ and Co, instead of the electrochemical reduction/oxidation of hydrogen atoms on the electrode surface [12].

CNTs have been demonstrated to exhibit high electrical conductivity and good mechanical properties. CNTs are also chemically stable and have very large accessible surface area. It is hopeful to improve the electrochemical properties of alkaline rechargeable batteries with the addition of CNTs. Many efforts have been done on this purpose [14–18]. However, to the best of the author's knowledge, there is no report on the electrochemical performance of Co-CNT composites.

In this work, Co-CNT composites are prepared via a ball-milling process. In order to achieve an optimized result of decreased Co particles and undestroyed structure of CNTs, a moderate ball-milling time of 10 h is chosen. Their electrochemical behaviors and the mechanism of electrochemical reaction are primarily investigated.

2. Experiment

2.1. Preparation and structural characterization

Co (purity, >99.0%) and CNTs (purity, >95%) were procured from Tianjin Kermel Chemical Reagent Co. Ltd and Shenzhen Nanotech Port Co. Ltd, respectively. Both of the reagents were used without further treatment. All samples, including pure Co and Co-CNT composites mixing at the weight ratios of 4/1, 5/1, 6/1, and 7/1, respectively, were ball-milled using a planetary ball mill (ZKX-2B, Nanjing) in a stainless steel vessel under Ar atmosphere at a speed of 450 rpm for 10 h. The ball-to-powder weight ratio was 20/1. All samples were characterized by X-ray diffraction (XRD, Rigaku D/max-2500). The morphology and chemical state

* Corresponding author. Tel.: +86 22 23498089; fax: +86 22 23502604.
E-mail address: jiaolf@nankai.edu.cn (L. Jiao).

0378-7753/$ – see front matter © 2010 Elsevier B.V. All rights reserved.
doi:10.1016/j.jpowsour.2010.11.145

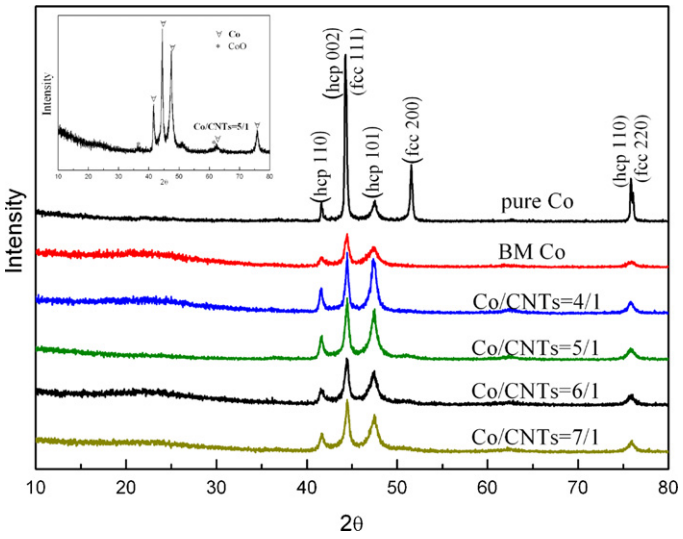

Fig. 1. XRD patterns of pure Co, ball-milled Co and Co-CNT composites with different Co/CNT weight ratios.

were investigated with transmission electron microscopy (TEM, Tacnai 20) and X-ray photoelectron spectroscopy (XPS, Kratos Axis Ultra DLD multi-technique), respectively.

2.2. Electrochemical measurements

Negative electrodes were constructed through mixing as-prepared materials with carbonyl nickel powders in a weight ratio of 1/3. The powder mixture was pressed under 30 MPa of pressure into a small pellet of 10-mm diameter and 1.5-mm thickness. The pellet was then pressed under 20 MPa of pressure between two pieces of Ni foam.

Electrochemical measurements were conducted in a three-compartment cell using pure Co and Co-CNT composites as working electrodes, $NiOOH/Ni(OH)_2$ and Hg/HgO electrodes were used as the counter electrode and the reference electrode, respectively. The electrolyte solution was a 6-M KOH aqueous solution.

The cycle life and charge–discharge curves were tested by a LAND battery-test instrument (CT2001A). The negative electrodes were charged at a current density of 100 mA g^{-1} for 5 h, and then discharged to −0.5 V (vs. Hg/HgO) at a current density of 25 mA g^{-1} after resting for 5 min at room temperature. Zahner IM6ex electrochemical workstation is used for cyclic voltammetry (scan rate: 0.2 mV s^{-1}; potential interval: −1.2 to −0.4 V vs. Hg/HgO) and linear polarization (scan rate: 0.1 mV s^{-1}; potential interval: −6 to 6 mV vs. open circuit potential).

To study the electrochemical reaction mechanism, the microstructure of the ball-milled Co-CNT composites after different cycles was measured by XRD. In order to avoid the influence of the Ni diffraction peaks, the electrodes for XRD measurement were prepared by mixing Co-CNT powders, acetylene black and polytetrafluoroethylene at the weigh ratio of 10:2:1 into a paste, which was roll pressed to 0.15-mm thick film and then pressed onto a porous nickel mesh. After electrochemical cycles, the samples at different discharged and charged states for XRD measurements were washed with distilled water and ethanol, and dried in vacuum at 80 °C for 3 h.

3. Results and discussion

3.1. Characterization of structure and morphology of Co-CNT composites

Fig. 1 shows the XRD patterns of pure Co, ball milled Co and Co-CNT composites with different Co/CNT weight ratios. As shown in Fig. 1, the original Co powders display almost a pure fcc phase (JCPDS 15-806) except for a small amount of hcp phase (JCPDS 5-727). After ball-milling, most peaks of hcp phase transform to fcc phase. In addition, all diffraction peaks of ball-milled Co and Co-CNT composites are broadened and weakened, indicating the formation of nanocrystalline Co during the ball-milling process. Most of the peaks of ball-milled Co-CNT composite can be indexed to Co except a small amount of CoO. Possibly because the ball milling time is relatively short in our study, we could not find the formation of any cobalt carbides.

Typical TEM images of the ball-milled Co-CNT composites (Co/CNTs = 5/1, BM 10 h) are illustrated in Fig. 2. It can be seen that the cobalt nanoparticles with the size between 50 and 100 nm are well dispersed throughout the CNT amorphous network. The CNTs are cut shorter with open ends. Some of them entangle together on the surface of Co particles, leading to a coating layer among them.

3.2. Electrochemical performance of Co-CNT composites

Fig. 3 shows the cycle stability of pure Co, ball-milled Co, CNTs and Co-CNT electrodes at a discharge current density of 25 mA g^{-1}. As it can be seen, the CNTs we used here can be regarded as an inactive matrix. After ball-milling, the discharge capacities of Co

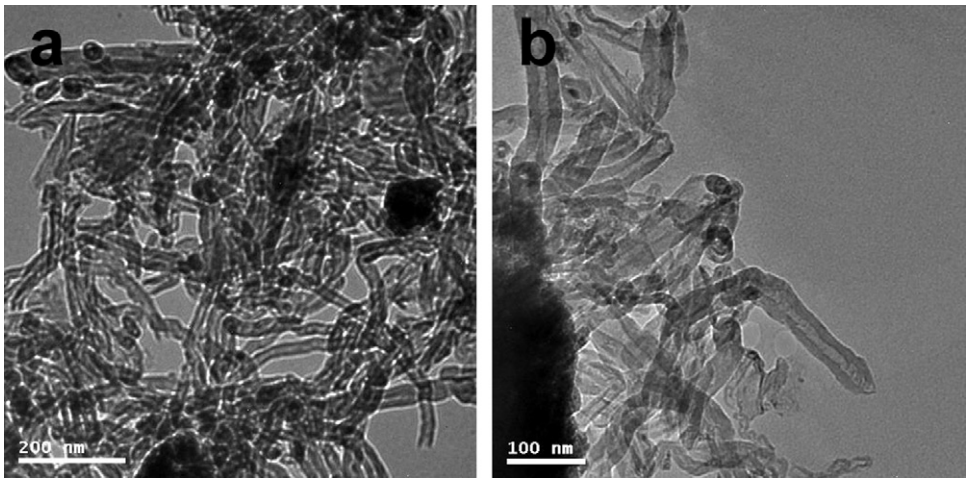

Fig. 2. TEM images of Co-CNT composite (Co/CNTs = 5/1, BM 10 h).

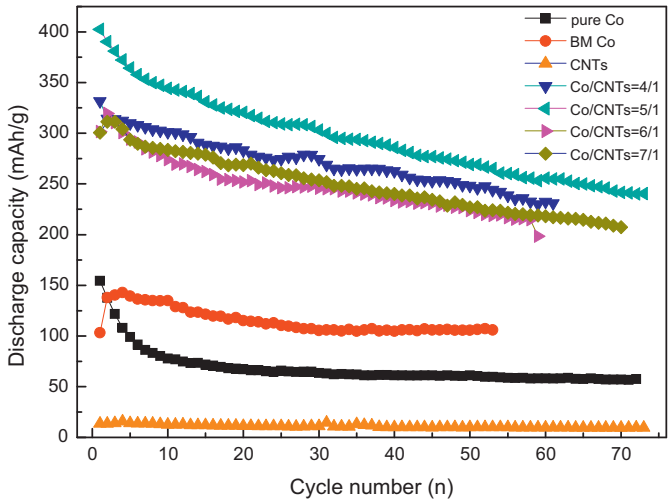

Fig. 3. Cycle performance of pure Co, ball-milled Co, CNTs and Co-CNT composite electrodes with different weight ratios.

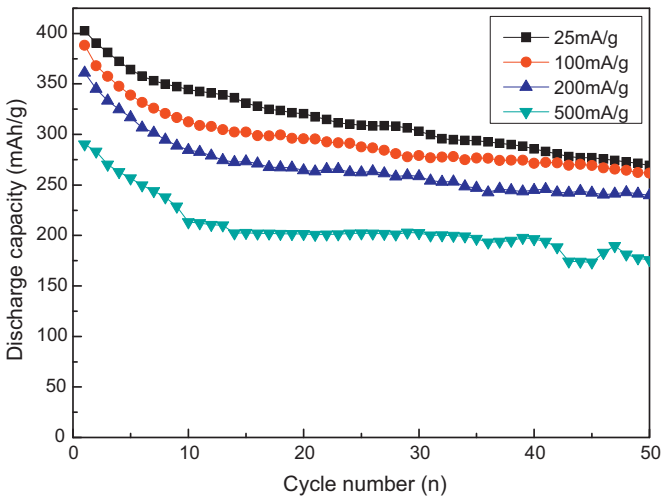

Fig. 4. Cycle performance of the Co-CNT composite (weight ratio 5/1, BM 10 h) electrode at different discharge current densities.

and Co-CNT composites are all increased to some extent. Especially for Co-CNT composite (weight ratio 5/1, BM 10 h) electrode, the maximum discharge capacity can reach 402.5 mAh g^{-1} during the first cycle. After 50 cycles, the discharge capacity can still remain at 270 mAh g^{-1}. Many factors contribute to it. Through ball-milling, the size of Co particles decreases, also the CNTs are cut short, both of which lead to higher electrochemically accessible surface area. As we know, larger contact area with alkaline solution is in favor of the surface electrochemical redox [19]. Besides, CNTs possess high electronic conductivity and useful mechanical properties, which can prevent inner resistance from raising so as to keep the good cycle performance of the ball-milled composite electrode [16]. In addition, the phase transformation of Co from hcp to fcc increases the reaction activity, causing a larger discharge capacity [20].

However, the discharge capacities of these composite electrodes vary with the mixing rate of Co and CNTs. This is probably due to the nature of CNTs. According to the report of Zhang et al. [16], adding too many CNTs is not helpful to the performance of batteries, which would cause the decreasing of the active material density in stainless net of negative electrode due to CNTs holding large volume.

To investigate the kinetic characteristics of the electrodes, the rate capability and cycling ability were measured at different discharge current densities. Fig. 4 shows the cycle performance of the Co-CNT composite (weight ratio 5/1, BM 10 h) electrode at the current densities 25, 100, 200 and 500 mAh g^{-1}. As it is shown, the reversible discharge capacity decreases in a certain degree with the current density increasing, which is consistent with the traditional view [7]. On the other hand, it can be seen that the effect of high current density on the cycle life of the electrode is small, so the electrode has good kinetic performance. This can also be attributed to the larger reaction surface of the electrode with the addition of CNTs, which increases the electrochemical reaction surface of the active particles. Thus, the good conductive property of CNTs with stable electrochemical properties is of importance for providing enough current collectors in the electrodes, thus decreasing the charge transfer resistance [15]. This can be confirmed by the result of exchange current density obtained from Fig. 5.

The exchange current density I_0, which is the rate of the charge-transfer reaction, can be obtained according to the following formula: $I_0 = RTI/F\eta$, where R is the gas constant, T is the absolute temperature (K), I is the applied current density (mA g^{-1}), F is the Faraday constant and η is the total overpotential (mV). The linear polarization curves for pure Co and Co-CNT composite are shown in Fig. 5 and the calculated I_0 values are 17.95 and 94.23 mA g^{-1} for pure Co and Co-CNT composite (weight ratio 5/1, BM 10 h), respectively. It is clear that the value of I_0 is increased significantly after the modifications. This result certifies that the rate of charge transfer reaction on the alloy surface is greatly improved, hence reducing the overpotential during the discharge process and leading to an increase of discharge capacity of the electrode.

3.3. The mechanism of electrochemical reaction

As shown in Fig. 6b, the Co-CNT composite is discharged directly without the first charging process. When comparing it to Fig. 6a, it is noted that the discharge potential plateau is close to that charged first shown in Fig. 6a. The discharge capacity of the uncharged Co-CNT composite can reach 316.5 mAh g^{-1} in the first cycle. According to Chung et al. [20], Co may react as a negative electrode in the Ni-MH battery in two formats: (1) $Co + xH_2O \rightarrow CoH_x + xOH^-$ and (2) $Co(OH)_2 + 2e \rightarrow Co + 2OH^-$. In the former reaction, the measured maximal discharge capacity for pure crystalline Co powder is 428 mAh g^{-1}, while that in the latter reaction is normally not more than 80 mAh g^{-1} [20]. As shown in Fig. 6b, because the sample was not charged before discharge, the high discharge capacities did not result from the dehydrogenation reaction of CoH_x distinctly. Thus,

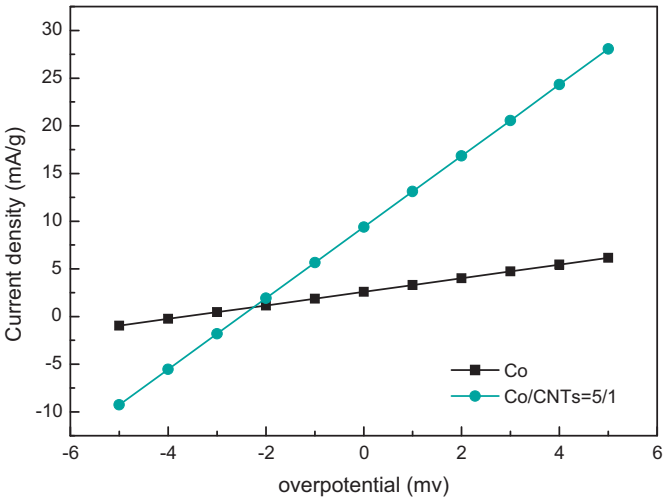

Fig. 5. Linear polarization curves of original Co and Co-CNT composite (weight ratio 5/1, BM 10 h).

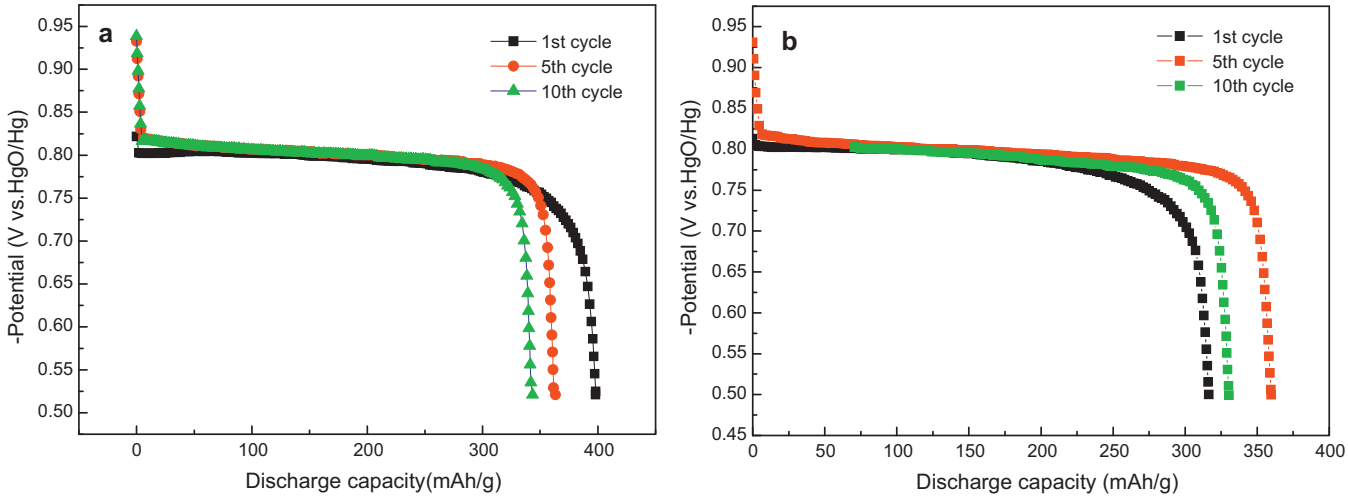

Fig. 6. Discharge curves of Co-CNT composite (weight ratio 5/1, BM 10 h): (a) charged in the first cycle; (b) discharged directly in the first cycle.

it seems that the faradaic reaction of $Co/Co(OH)_2$, i.e. the electron loss due to the cobalt oxidation, should contribute to the discharge capacities. However, the discharge capacity of the sample has great discrepancy with the one charged first. To examine the difference, Co2p core level spectra of the Co-CNT composite (weight ratio 5/1, BM 10 h), before and after Ar sputtering, are recorded in Fig. 7. The cobalt exists as CoO (781 eV) on the surface of this sample before Ar sputtering, due to the surface oxidation of active Co nanoparticles in air, which is in agreement with the result of XRD patterns enclosed in Fig. 1. The characteristic Co2p peak is shifted from 781 eV to 778.1 eV after Ar sputtering for 10 min, suggesting the existence of metallic Co in the bulk phase of the composite. Thus, it is inferred that these oxidized species on the surface of the Co-CNT composite are first reduced to Co and subsequently also oxidized to $Co(OH)_2$. Hence the increased capacity is observed in the first cycle of a pre-charged sample. All electrodes have similar potential changes in the following cycles, indicating that the faradaic reaction is dominated in the Co-CNT composite.

Cyclic voltammogram curves of pure Co, ball-milled Co and Co-CNT composite (weight ratio 5/1, BM 10 h) at a scan rate of 2 mV s^{-1} are presented in Fig. 8. A pair of remarkable cathodic and anodic current peaks can be found for each CV curve. It is apparent that the integral peak area of Co-CNT composite (weight ratio 5/1, BM 10 h) is larger than that of pure Co and ball-milled Co, indicating that the electrocatalytic activity of Co-CNT composite (weight ratio 5/1, BM 10 h) is the best. The oxidation peak is located at the potential of −0.72 V (vs. Hg/HgO) in the anodic process, which can be assigned to the oxidation reaction of Co [4,11]. There is no other peaks observed in the anodic process, so the conversion reaction of $Co/Co(OH)_2$ is dominant on Co-CNT composite and it offers most of the discharge capacity.

In order to further confirm the reaction mechanism mentioned above, XRD patterns of the Co-CNT composite (weight ratio 5/1, BM 10 h) at different charge and discharge states are illustrated in Fig. 9. It can be found that only the diffraction peaks of metallic Co are detected at the fully charged state in the first cycle, which are almost identical to those of the as-prepared Co-CNT composite. At the fully discharged state in the first cycle, most of the diffraction peaks can be indexed as $Co(OH)_2$ and the diffraction peaks of the metallic Co become weak. The $Co(OH)_2$ phase is still detected as the coexisting phase with metallic Co at the fully charged state. It means that only partial metallic Co in the Co-CNT composite is involved in the faradaic reaction, resulting in the low utilization of the active Co. In addition, the diffraction intensity of $Co(OH)_2$ increases gradually to some extent at the fully discharged state, implying that the redox irreversibility of metallic Co increases gradually during cycling. The Co peaks are poorly crystalline with abundant defects induced during the ball-milling process. Whereas

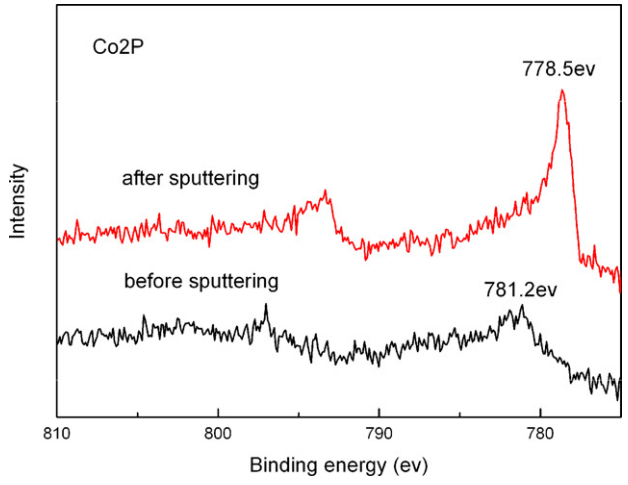

Fig. 7. Co2p core level spectra of the Co-CNT composite (weight ratio 5/1, BM 10 h) before and after Ar sputtering for 10 min.

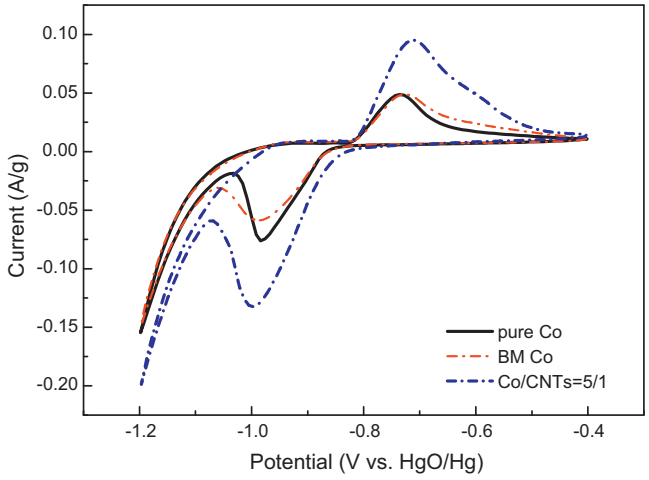

Fig. 8. Cyclic voltammogram curves of pure Co, BM Co and Co-CNT composite.

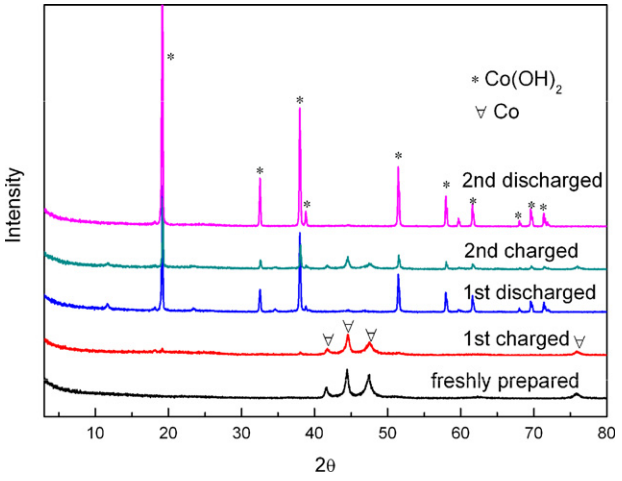

Fig. 9. XRD patterns of the Co-CNT composite electrode (weight ratio 5/1, BM 10 h).

the $Co(OH)_2$ shows a good crystallinity, which is formed during the slow dissolution–precipitation process of Co nanoparticles in alkaline solution. Based on the analyses above, we can attribute the discharge capacity of Co-CNT sample to the redox reaction between Co and $Co(OH)_2$.

4. Conclusion

The Co-CNT composites were prepared by ball-milling cobalt and CNTs mixing with different weight ratios for 10 h. Because of the predominant properties of CNTs and synergetic impact of Co and CNTs through ball-milling, the electrochemical performance of Co-CNT electrodes is significantly improved than that of pure Co electrode. Among them, the Co-CNT electrode (Co/CNTs = 5/1, BM 10 h) shows the highest initial discharge capacity (402.5 mAh g^{-1}), good retention rate and better kinetic performance under high discharge current density, which is a promising candidate as negative electrode material for alkaline rechargeable batteries. Based on the analyses of TEM, XPS and electrochemical performance, it is found that the formation of Co nanoparticles with a good reactivity and CNT network with high electrochemical conductivity and larger contact area with alkaline solution are responsible for the high initial discharge capacities of the samples. Most of the discharge capacity can be attributed to the redox reaction between Co and $Co(OH)_2$.

Acknowledgements

This work was financially supported by NSFC (50631020, 50701025, 50971071, 51071087), 863 Program (2007AA05Z149, 2007AA05Z108), 973 Program (2010CB631303), MOE Innovation Team(IRT0927) and Doctoral Foundation of Ministry of Education (20070055064).

References

[1] X.P. Gao, S.M. Yao, T.Y. Yan, Z. Zhou, Energy Environ. Sci. 2 (2009) 502–505.
[2] M.J. Aragón, B. León, C.P. Vicente, Chem. Mater. 21 (2009) 1834–1840.
[3] J.L. Fernández, V. Raghuveer, A. Manthiram, J. Am. Chem. Soc. 127 (2005) 13100–13101.
[4] Y. Wang, J.M. Lee, X. Wang, Int. J. Hydrogen Energy 35 (2010) 1669–1673.
[5] Y.D. Wang, X.P. Ai, H.X. Yang, Chem. Mater. 16 (2004) 5194–5197.
[6] D.W. Song, Y.J. Wang, Y.P. Wang, L.F. Jiao, H.T. Yuan, Electrochem. Commun. 10 (2008) 1486–1489.
[7] Y.L. Cao, W.C. Zhou, X.Y. Li, X.P. Ai, X.P. Gao, H.X. Yang, Electrochim. Acta 51 (2006) 4285–4290.
[8] G. He, L.F. Jiao, H.T. Yuan, Y.Y. Zhang, Y.J. Wang, Electrochem. Commun. 8 (2006) 1633–1638.
[9] Y.H. Zhang, L.F. Jiao, H.T. Yuan, Y.Y. Zhang, L. Liu, Y.J. Wang, Int. J. Hydrogen Energy 33 (2008) 1317–1322.
[10] Z.W. Lu, S.M. Yao, G.R. Li, T.Y. Yan, X.P. Gao, Electrochim. Acta 53 (2008) 2369–2375.
[11] S.M. Yao, K. Xi, G.R. Li, X.P. Gao, J. Power Sources 184 (2008) 657–662.
[12] P. Elumalai, H.N. Vasan, N. Munichandraiah, J. Power Sources 93 (2001) 201–208.
[13] Q.S. Chen, S.G. Sun, J.W. Yan, J.T. Li, Z.Y. Zhou, Langmuir 22 (2006) 10575–10583.
[14] S.P. Yi, H.Y. Zhang, L. Pei, S. Hu, L.C. Hu, Mater. Sci. Eng. B 128 (2006) 125–129.
[15] J. Lv, J.P. Tu, W.K. Zhang, J.B. Wu, H.M. Wu, B. Zhang, J. Power Sources 132 (2004) 282–287.
[16] H.Y. Zhang, Y.T. Chen, Q.F. Zhu, G.Q. Zhang, Y.M. Chen, Int. J. Hydrogen Energy 33 (2008) 6704–6709.
[17] S. Li, G.L. Pan, Y. Zhang, X.P. Gao, J.Q. Qu, J. Yan, J. Alloys Compd. 353 (2003) 295–300.
[18] Y. Wang, W.Q. Deng, X.W. Liu, S.Y. Wang, X. Wang, Int. J. Hydrogen Energy 34 (2009) 1444–1449.
[19] D.W. Song, Y.J. Wang, Q.H. Wang, Y.P. Wang, L.F. Jiao, H.T. Yuan, J. Power Sources (2010), doi:10.1016/j.jpowsour.2010.04.088.
[20] S.R. Chung, K.W. Wang, T.P. Perng, J. Electrochem. Soc. 153 (2006) A1128–A1131.